

## BRIGHT POINTS IN THE INTER-NETWORK QUIET SUN

J. SÁNCHEZ ALMEIDA<sup>1</sup>, I. MÁRQUEZ<sup>1,2</sup>, J. A. BONET<sup>1</sup>, I. DOMÍNGUEZ CERDEÑA<sup>3</sup>, AND R. MULLER<sup>4</sup>

*Draft version December 12, 2018*

### ABSTRACT

High resolution G-band images of the interior of a supergranulation cell show ubiquitous Bright Points (some 0.3 BPs per Mm<sup>2</sup>). They are located in intergranular lanes and often form chains of elongated blobs whose smallest dimension is at the resolution limit (135 km on the Sun). Most of them live for a few minutes, having peak intensities from 0.8 to 1.8 times the mean photospheric intensity. These BPs are probably tracing intense magnetic concentrations, whose existence has been inferred in spectro-polarimetric measurements. Our finding provides a new convenient tool for the study of the inter-network magnetism, so far restricted to the interpretation weak polarimetric signals.

*Subject headings:* Sun: magnetic fields – Sun: photosphere

### 1. INTRODUCTION

The presence of Bright Points (BPs) in the solar photosphere was first reported by Dunn & Zirker (1973) and Mehlretter (1974). They were identified with small magnetic concentrations, which are expected to be bright (Spruit 1977)<sup>5</sup>. BPs appear in all magnetic structures: around sunspots, in plage regions, and in the network (e.g. Muller 1994). This Letter shows how they are also very common inside supergranulation network cells.

The new result refers to the magnetism of the so-called Inter-Network (IN), and may be consequential. The seemingly inactive IN provides a large fraction of the (unsigned) magnetic flux and energy existing on the solar surface at any given time (e.g., Stenflo 1982; Sánchez Almeida 2003b, 2004; Trujillo Bueno et al. 2004). Therefore, it may be an important element to understand the global magnetic properties of the Sun (e.g., the structure of the quiet corona, Schrijver & Title 2003; the chromospheric heating, Goodman 2004; the sources of the solar wind, Woo & Habbal 1997; Hu et al. 2003; or the emergence of magnetic flux, De Pontieu 2002). We still have a very primitive knowledge of the properties of the IN fields, which mostly comes from the model-dependent analysis of weak spectro-polarimetric signals (for a recent review, see Sánchez Almeida 2004). The finding of G-band BPs provides a new simple and direct mean to study the IN magnetism using unpolarized light. In addition, the presence of BPs strongly suggests that part of the IN fields have kG field strengths. Spectro-polarimetric observations indicate IN field strengths going all the way from zero to kG (see, e.g., the introduction of Sánchez Almeida et al. 2003). The presence of kG field strengths has been particularly controversial, and this work provides independent support.

### 2. OBSERVATIONS AND IMAGE RESTORATION

A quiet Sun IN region was observed at the solar disk center with the SST (Swedish Solar Telescope), a new 1-m instrument equipped with adaptive optics (Scharmer et al. 2003a,b). The Field-Of-View (FOV) was selected using Ca II H images to avoid network magnetic concentrations. We image through a 10.8 Å wide filter centered in the G-band at 4305.6 Å. Although magnetic concentrations are bright at all wavelengths, they become particularly conspicuous in this CH band (Muller & Roudier 1984; Berger et al. 1995). The optical setup included a Phase Diversity (PD) device for post-facto restoration of the optical aberrations induced by the terrestrial atmosphere and the telescope (Gonsalves & Childlaw 1979; Paxman et al. 1992). The series of PD images was taken on September 30, 2003, from 11:33 UT to 12:23 UT. We use a 10-bit Kodak Megaplug 1.6 camera (pixel size 0.''041, exposure time 8 msec). Real-time frame selection provided us with the 4 sharpest images every 20 sec, which are needed in our PD inversion code (Bonet & Márquez 2003, based on Löfdahl & Scharmer 1994, and Paxman et al. 1996). First, each image of the series is divided in a mosaic of 96 overlapping isoplanatic patches, which we restore independently. Then the mosaic is assembled, and the 4 images of each selection interval are combined to form a restored snapshot. The process of splitting, restoring and merging renders a FOV of 23''x 35''; see Fig. 1. Excellent and rather bad moments of seeing alternated during the observing run. Therefore several sets of 4 images could not be successfully restored, leaving gaps in our series. It finally has 100 restored snapshots during its 50 min duration. The PD code includes a self-regulated high-spatial-frequency noise removal filter. Given the conditions of the data, the largest cutoffs set by this filter are 0.''14, i.e., only slightly worst than the diffraction limit (0.''09). Note that the cutoff differs for each PD restoration, and so, it varies within a single restored snapshot. The cutoff approximately yields the Full Width Half Maximum (FWHM) of the point spread function, a rule of thumb used in § 3.2.

Ca images allowed us to center the G-band FOV within a supergranulation cell. Figure 2a shows one of these Ca images, which includes a box with the G-band FOV outline. Note how the brightest Ca patches remain outside the G-band contour. Only a small patch in the lower right corner lies within the bounds. In order to stress the IN character of our target, we pinpoint the observed FOV in a full disk MDI mag-

<sup>1</sup> Instituto de Astrofísica de Canarias, E-38205 La Laguna, Tenerife, Spain; jos@iac.es, imr@iac.es, jab@iac.es.

<sup>2</sup> Departamento de Análisis Matemático, Universidad de La Laguna.

<sup>3</sup> Universitäts-Sternwarte, Geismarlandstraße 11, D-37083 Göttingen, Germany; ita@uni-sw.gwdg.de.

<sup>4</sup> Observatoire Midi-Pyrenees, 14 Avenue Edouard Belin, 31400 Toulouse, France; muller@bagn.obs-mip.fr.

<sup>5</sup> The highly magnetized plasma of a magnetic concentration is more transparent than the mean photosphere, allowing photons to escape from deep (and usually) hot sub-photospheric layers.

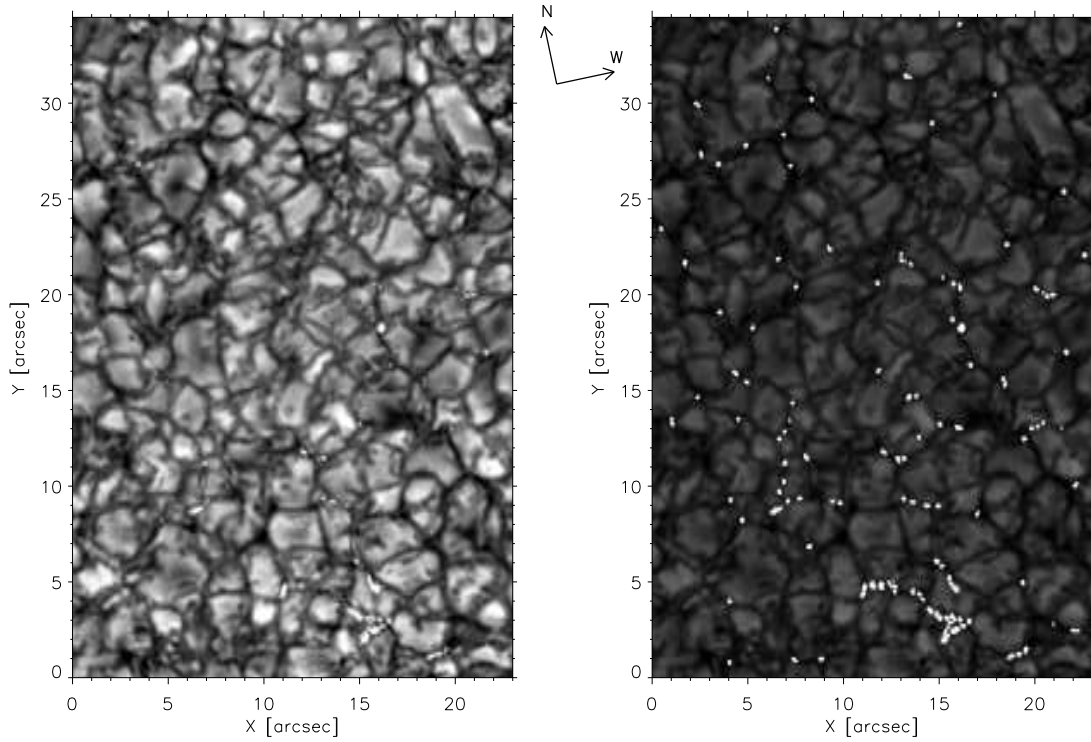


FIG. 1.— Left: snapshot used for in-depth analysis. Right: same snapshot with lower contrast and the position of the selected BPs marked in white. The axes are in arcsec from the lower left corner. The arrows indicate the solar north and west directions during observation.

netogram<sup>6</sup> taken 18 minutes before the beginning of the series. It is shown in Fig. 2b. The figure includes an inset with the SST Ca image of the region. Figure 2b was set up to emphasize the continuity between the MDI magnetogram and the Ca images, and so, it displays the unsigned polarimetric signals. Figure 2c shows the true MDI magnetogram saturated at  $\pm 50$  G to reveal the weakest network features. A small blob appears within the G-band FOV. The rest remains field-free as far as the MDI magnetogram is concerned. The MDI signals within the FOV are  $(-0.9 \pm 7.1)$  G, with the standard deviation matching the MDI noise (e.g., 6.9 G for Hagenaar 2001). The magnetic patch of the MDI magnetogram is very conspicuous in the G-band; see the conglomerate of BPs at the lower right part of Fig. 1, coordinates  $[16'', 3'']$ .

### 3. ANALYSIS AND RESULTS

#### 3.1. Area coverage and number density

The sharpest snapshot of the time series was selected for in-depth study (Fig. 1, left). Although this reference snapshot was chosen by visual inspection, it has one of the largest contrasts of the full series (14.3%). Then, playing the series back and forth, we single out all those BPs which (a) were in the reference snapshot, (b) persisted three or more snapshots, and (c) stay in an intergranular lane. This subjective selection of BPs was complemented with an automatic determination of their areas. We apply the segmentation algorithm by Strous (1994, Chapter 8), and then those patches overlaying a visually selected BP were chosen as the area of the

BP. The result is shown in Fig. 1, right. We identify 126 individual points, some of which are part of long chains. Given the area of the FOV, we detect 0.3 points per  $\text{Mm}^2$ . The density of BPs increases towards the lower left part of the FOV (Fig. 1), i.e., when approaching the network patch (Fig. 2c). The area associated with these BPs covers some 0.5% of the FOV. This area depends on the segmentation algorithm, and a more meaningful estimate is carried out in § 3.2.

#### 3.2. Size and Brightness

The BPs stay in intergranular lanes, which are narrow dark wells of the intensity distribution. Title & Berger (1996) show how this fact biases any measurement of size unless the shape of the background is considered. They propose a 2-Gaussian fit to decontaminate from the influence of the intergranular background. We adopt this approach for estimating the widths of our BPs. Those pixels selected by the segmentation algorithm were fitted using

$$\begin{aligned}
 f &= c + aG(x, y, x_0, y_0, \sigma_x, \sigma_y, \theta) - bG(x, y, x_0, y_0, \sigma'_x, \sigma'_y, \theta), \\
 G(x, y, x_0, y_0, \sigma_x, \sigma_y, \theta) &= \exp(-(r_x^2 + r_y^2)), \\
 r_x &= [(x - x_0) \cos \theta + (y - y_0) \sin \theta] / \sigma_x, \\
 r_y &= [-(x - x_0) \sin \theta + (y - y_0) \cos \theta] / \sigma_y.
 \end{aligned} \tag{1}$$

The 2-Gaussian function  $f$  depends on the spatial coordinates  $x$  and  $y$ , as well as on 10 free parameters:  $a$ ,  $b$ , and  $c$  for the amplitudes of two Gaussians and a background,  $x_0$  and  $y_0$  for the core of the BP,  $\theta$  for a global orientation,  $\sigma_x$  and  $\sigma_y$  for the widths of the BP and, finally,  $\sigma'_x$  and  $\sigma'_y$  for the widths of the intergranular lane. By means of a non-linear least squares algorithm, we tried to reproduce to all BPs selected in Sec.3.1.

<sup>6</sup> <http://soi.stanford.edu>

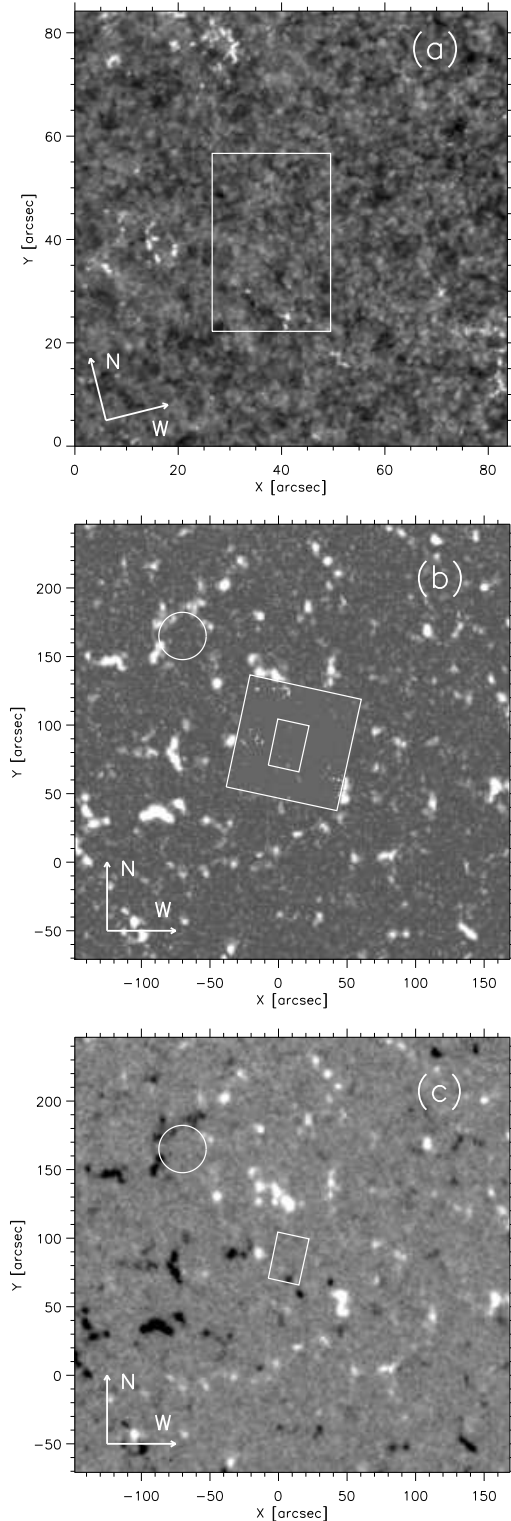


FIG. 2.— (a) Ca II H image corresponding to the reference G-band snapshot. The position of the G-band FOV within this larger Ca image is marked by the box. Axes are in arcsec from the lower left corner. (b) Absolute value of an MDI magnetogram taken right before the observation. The inset corresponds to the Ca image in (a), and it reveals MDI network patches continuing within the SST Ca image. Axes are in arcsec from the solar disk center. The circle shows the typical size of a supergranulation cell. (c) Section of the MDI magnetograms scaled between  $\pm 50$  G. The box corresponds to the G-band FOV.

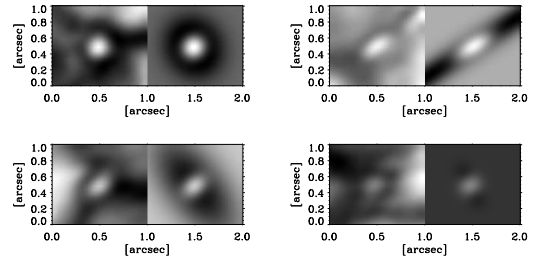


FIG. 3.— Four representative pairs of 2-Gaussian fits (right) and the corresponding observed G-band BPs (left).

Some 60% of the trials converged. Figure 3 shows four representative cases, which indicate how the elliptical contours of the 2-Gaussian functions really reproduce the observed BP shapes.

Figure 4a contains the histograms of the FWHM of the 2-dimensional Gaussians representing the BP (FWHM =  $1.67\sigma_x$  or  $1.67\sigma_y$ ). The minor axis FWHM peaks at some 135 km, and it seldom exceeds 200 km. We believe that this 135 km represents the mean spatial resolution of the snapshot. As we discuss in § 2, the resolution varies along the FOV, with a lower limit of some  $0''.14$  or 100 km. The width of the minor axis histogram is mostly set by uncertainties in the non-linear least squares fit (some 30 km, as provided by the fitting routine).

The interpretation of the areas derived in § 3.1 is ambiguous. We prefer a straight definition based on the 2-Gaussian fits, namely, the area within the elliptical contour embraced by the FWHM (i.e.,  $2.18\sigma_x\sigma_y$ ). This definition yields areas 40% larger than the segmentation algorithm. Then the 0.5% coverage in § 3.1 turns out to be 0.7%.

Figure 4b shows a scatter plot of the peak G-band intensity (i.e.,  $a - b + c$  in Eq. [1]) versus minor axis FWHM. There is no obvious correlation between brightness and size, which can be interpreted as the unresolved character of most of the features (e.g., Berger et al. 1995). Figure 4b also shows many BPs with an intensity smaller than that of the mean photosphere. On top of this, a few BPs reach 1.8 (close but still below the expected intensity for a fully resolved magnetic concentration; Kiselman et al. 2001; Sánchez Almeida et al. 2001; Steiner et al. 2001; Schüssler et al. 2003). In a different snapshot of the series, the network clump peak intensity scores 2.3.

### 3.3. Lifetimes

Lifetimes were estimated by visual inspection of the time series. The BPs in the reference snapshot were visually tracked to find out when they appear and disappear. This time interval defines the lifetime. A histogram of lifetimes is represented in Fig. 4c, the solid line. Most lifetimes are shorter than 10 min. In addition, some BPs live as much as we can measure (longer than 30 min). Keep in mind that the lifetimes are strongly biased. First, BPs often appear or end within one of the gaps of the time series, which underestimate the true values. Second, the detection criteria bias the estimates towards long-lasting BPs (§ 3.1). Although these caveats should be kept in mind, we believe that most BPs are really short-lived. Figure 4c, the dotted line, shows a histogram based on BPs whose birth and death we witnessed, and they have short lifetimes.

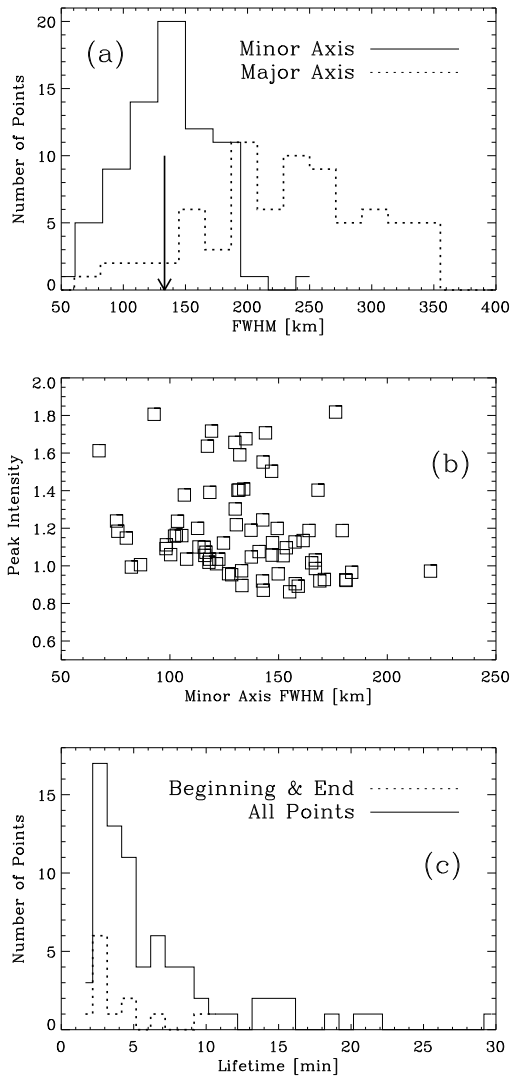


FIG. 4.— (a) Histograms of the G-band BP FWHM obtained from the 2-Gaussian fits. The mean FWHM along the minor axis is 135 km (see the arrow on the figure), which we interpret as the spatial resolution of the observation. (b) Peak intensity versus FWHM. No obvious correlation exists. The intensities are refereed to the mean photosphere. (c) Histograms of G-band BP lifetimes. The dotted line is based on those BPs whose beginning and end we witnessed.

#### 4. COMMENTS AND CONCLUSIONS

We have detected many Bright Points (BPs) in the interior of a supergranulation cell (i.e., in the Inter-Network or IN). According to the current paradigm, these bright points trace intense magnetic concentrations (§ 1). Our finding has two main consequences. First, it provides a new convenient tool for the study of the IN magnetism, so far restricted to the interpretation of low spatial resolution weak polarimetric signals. Second, it supports a result based on Zeeman magnetometry indicating that part of the IN magnetic fields are not weak but have kG magnetic field strengths (Sánchez Almeida & Lites 2000; Socas-Navarro & Sánchez Almeida 2002, 2003). The same polarimetric measurements also point out how these kG concentrations carry the body of the IN magnetic flux and energy (Sánchez Almeida et al. 2003; Sánchez Almeida 2004). Consequently, unpolarized imaging may allow us to detect and study a significant fraction of the IN magnetism.

The detected BPs cover some 0.7% of the surface, which is not enough to account for the magnetic signals found by (Domínguez Cerdeña et al. 2003a, 2003b, Sánchez Almeida 2003a). Several reasons may explain this difference. We miss many BPs since the detectability critically depends on the resolution (Title & Berger 1996), and our BPs remain unresolved (§ 3.2). On the other hand, some strong fields may not be bright. The actual brightness depends on subtleties of the magnetic concentration and its non-magnetic environment, and sometimes modeling shows faint kG features (Sánchez Almeida et al. 2001). Yet another possibility is the random fluctuation of properties of different cell interiors.

The work was funded by the Spanish project AYA2001-1649 and the EC contract HPRN-CT-2002-00313. Thanks are due to F. Kneer for continuous support, and to A. Sainz Dalda for help with MDI data (courtesy of the SOHO/MDI consortium by ESA & NASA). The SST is operated by the Institute for Solar Physics, Stockholm, at the ORM of the IAC.

#### REFERENCES

- Berger, T. E., Schrijver, C. J., Shine, R. A., Tarbell, T. D., Title, A. M., & Scharmer, G. 1995, *ApJ*, 454, 531
- Bonet, J. A., & Márquez, I. 2003, in *ASP Conf. Ser.*, Vol. 307, *Solar Polarization 3*, ed. J. Trujillo-Bueno & J. Sánchez Almeida (San Francisco: ASP), 137
- De Pontieu, B. 2002, *ApJ*, 569, 474
- Domínguez Cerdeña, I., Kneer, F., & Sánchez Almeida, J. 2003a, *ApJ*, 582, L55
- Domínguez Cerdeña, I., Sánchez Almeida, J., & Kneer, F. 2003b, *A&A*, 407, 741
- Dunn, R. B., & Zirker, J. B. 1973, *Sol. Phys.*, 33, 281
- Gonsalves, R. A., & Childlaw, R. 1979, in *Proc. Soc. Photo-Opt. Instrum. Eng.*, Vol. 207, *Applications of Digital Image Processing III*, ed. A. G. Tescher, 32
- Goodman, M. L. 2004, *A&A*, in press
- Hagenaar, H. J. 2001, *ApJ*, 555, 448
- Hu, Y. Q., Habbal, S. R., Chen, Y., & Li, X. 2003, *J. Geophys. Res.*, 108(A10), 1377
- Kiselman, D., Rutten, R. J., & Plez, B. 2001, in *IAU Symp.*, Vol. 203, *Recent Insights into the Physics of the Sun and Heliosphere*, ed. P. Brekke, B. Fleck, & J. B. Gurman (San Francisco: ASP), 287
- Löfdahl, M. G., & Scharmer, G. B. 1994, *A&AS*, 107, 243
- Mehlretter, J. P. 1974, *Sol. Phys.*, 38, 43
- Muller, R. 1994, in *Solar Surface Magnetism*, ed. R. J. Rutten & C. J. Schrijver, NATO ASI Ser. 433 (Dordrecht: Kluwer), 55
- Muller, R., & Roudier, T. 1984, *Sol. Phys.*, 94, 33
- Paxman, R. G., Schulz, T. J., & Fienup, J. R. 1992, *JOSA*, A9, 1072
- Paxman, R. G., Seldin, J. H., Löfdahl, M. G., Scharmer, G. B., & Keller, C. U. 1996, *ApJ*, 466, 1087
- Sánchez Almeida, J. 2003a, *A&A*, 411, 615
- Sánchez Almeida, J. 2003b, in *AIP Conf. Proc.*, Vol. 679, *Solar Wind 10*, ed. M. Velli, R. Bruno, & F. Malara (New York: AIP), 293
- Sánchez Almeida, J. 2004, in *The Solar-B Mission and the Forefront of Solar Physics*, ed. T. Sakurai & T. Sekii, *ASP Conf. Ser.* (San Francisco: ASP), in press (astro-ph/0404053)
- Sánchez Almeida, J., Asensio Ramos, A., Trujillo Bueno, J., & Cernicharo, J. 2001, *ApJ*, 555, 978
- Sánchez Almeida, J., Domínguez Cerdeña, I., & Kneer, F. 2003, *ApJ*, 597, L177
- Sánchez Almeida, J., & Lites, B. W. 2000, *ApJ*, 532, 1215
- Schüssler, M., Shelyag, S., Berdyugina, S., Vögler, A., & Solanki, S. K. 2003, *ApJ*, 597, L173

- Scharmer, G. B., Bjelksjö, K., Korhonen, T. K., Lindberg, B., & Petterson, B. 2003a, Proc. SPIE, 4853, 341
- Scharmer, G. B., Dettori, P. M., Löfdahl, M. G., & Shand, M. 2003b, Proc. SPIE, 4853, 370
- Schrijver, C. J., & Title, A. M. 2003, ApJ, 597, L165
- Socas-Navarro, H., & Sánchez Almeida, J. 2002, ApJ, 565, 1323
- Socas-Navarro, H., & Sánchez Almeida, J. 2003, ApJ, 593, 581
- Spruit, H. C. 1977, Sol. Phys., 55, 3
- Steiner, O., Hauschildt, P. H., & Bruls, J. 2001, A&A, 372, L13
- Stenflo, J. O. 1982, Sol. Phys., 80, 209
- Strous, L. 1994, Ph.D. thesis, Utrecht University, Utrecht
- Title, A. M., & Berger, T. E. 1996, ApJ, 463, 797
- Trujillo Bueno, J., Shchukina, N. G., & Asensio Ramos, A. 2004, Nature, submitted
- Woo, R., & Habbal, S. R. 1997, Geophys. Res. Lett., 24, 1159